Sensors and Materials, Vol. 38, No. 3 (2026) 1591–1608
MYU Tokyo

S & M 4395

Development of Heat Stamping Die Through Optimization of Parameters for Defect Prevention

Qian Chen,[1] Jiayi Lu,[2*] Ye Li,[3] and Tian-Syung Lan[4]

[1]School of Art and Design, Wuhan University of Technology, Wuhan, Hubei 430070, China
[2]School of Digital Art and Design, Sichuan Technology and Business University, Chengdu, Sichuan 611745, China
[3]School of Information Science and Engineering, Weifang University of Science and Technology, Weifang, 262700, Shandong, China
[4]Department of Information Management, Yu Da University of Science and Technology, 168 Xuefu Rd, Zaoqiao 361, Miaoli, Taiwan

(Received December 15, 2025; accepted March 13, 2026)

Keywords: organizational performance, hot-formed parts, defect prevention and control

We optimized hot stamping process parameters for 2 mm boron steel (22MnB5) to enhance the mechanical properties and defect prevention of ultrahigh-strength steel components. Utilizing an orthogonal experimental design and numerical simulation, we analyzed the effects of heating temperature, holding time, and cooling water flow rate on the microstructural evolution and mechanical performance of the stamped parts. The results indicate that a heating temperature of 930 °C, a holding time of 4.5 min, and a water flow rate of ≥0.75 m/s must be maintained in the optimal process. Verification using these parameters presented a transformed, uniform lath martensitic microstructure with a tensile strength of 1535 MPa and a hardness exceeding 48 on the Rockwell C scale. By integrating a sensor monitoring system into the die design, process stability and tool safety can be ensured. By employing embedded piezoelectric force sensors to detect the volumetric expansion associated with the martensitic phase transformation and noncontact pyrometers for thermal history verification, the system enables a closed-loop control mechanism. This sensor-driven approach enables the precise, piece-by-piece optimization of quenching time, significantly preventing defects and ensuring the consistent quality of high-performance automotive components.

1. Introduction

High-speed steel (HSS) is widely used for cutting tools, such as drills, taps, and milling cutters, owing to its high toughness, hardness, wear resistance, heat resistance, and thermal stability.(1) By adding boron, hard phases, borides (compounds of boron with iron, chromium, titanium, or tungsten), are formed to further enhance HSS's thermal stability while reducing the manufacturing costs and energy consumption.(2,3) The hardness, wear resistance, and thermal stability of HSS are closely related to the characteristics of the martensitic matrix and the

*Corresponding author: e-mail: luhyuk@outlook.com
https://doi.org/10.18494/SAM6117

ISSN 0914-4935
https://myukk.org/

morphological distribution of the hard phases. In the hard phase, boron partially dissolves into the matrix, enhancing its hardness and the high-temperature wear resistance.

After centrifugal casting, borides form interconnected networks. This morphology reduces the continuity of the metallic matrix and leads to weak interfacial bonding between the hard phases and the matrix, resulting in poor overall compatibility and mechanical performance. Therefore, heat treatments, such as annealing, quenching, and multiple tempering processes, are required to improve the morphology and distribution of the hard phases and optimize the casting structure and properties.[4] Among the heat treatment methods, the quenching process has the largest impact on the structure and properties of HSS.[5] Fu *et al.* studied the effect of quenching temperature on HSS, finding that its hardness peaked when the matrix completely transformed at 1050 °C into martensite [a very hard microstructural phase of steel formed by rapid cooling (quenching)] from the face-centered cubic form of iron [(the austenite phase) that exists at high temperatures and plays a central role in heat treatment], but decreased at higher temperatures.[6] Kang and Lee observed the highest hardness of niobium-containing HSS rolls at 1050 °C.[7] Jung *et al.* indicated that hardness becomes highest at 1180 °C, but increasing the cooling rate suppressed martensitic transformation and increased the retained austenite phase.[8]

Although significant research has been conducted on the thermal parameters of quenching, the optimal conditions required to achieve maximum hardness in boron-containing HSS need further investigation, particularly regarding their consistent application in industrial environments. The difference in mechanical properties between rolled and quenched HSS is largely attributed to the enhanced hardenability imparted by boron; however, achieving these properties reliably requires precise control over the thermal history, which is difficult to maintain without advanced process monitoring. Consequently, there is a critical need to link process optimization with sensor technology to ensure that the strict cooling requirements for martensitic transformation are met during every cycle.

Therefore, we examined the effects of heating temperature, holding time, and cooling water flow rate on the microstructure and mechanical properties of 2 mm boron steel (22MnB5) to develop a hot stamping die integrated with a real-time sensor monitoring system. By optimizing these parameters and embedding piezoelectric force sensors and noncontact pyrometers into the die design, in this research, we sought to establish a closed-loop control mechanism that detects phase transformations and verifies thermal history in real time. The results contribute to the development of a uniform lath martensitic microstructure with superior strength, coupled with a sensor-based method for immediate defect prevention. The results contribute to the advancement of HSS production by demonstrating how intelligent sensing can be utilized to guarantee process stability and tool safety, ultimately leading to the zero-defect manufacturing of ultrahigh-strength components.

2. Methods

In this study, heating temperature, holding time, and cooling water flow rate were selected as the primary variables for optimization. While other factors, such as stamping pressure and transfer time, also influence the process, these three parameters are the most critical controllable

factors in a commercial hot stamping line and directly govern phase transformation.[9] Specifically, the heating temperature and holding time control the quality and homogeneity of the austenitization,[10] while the cooling water flow rate is the decisive factor in achieving the critical cooling rate required to ensure a fully martensitic microstructure in 22MnB5 boron steel.[11]

We utilized a cooling cycle test bench and a heating furnace to conduct a solid quenching orthogonal test. The material used was boron steel BR1500HS (2 mm thick), which has a full austenitization temperature (A_{c3}) of 811 °C. For the experimental setup, blanks of the boron steel measuring 150 × 30 mm^2 were cut from stamped parts, yielding a total of 48 samples that were split into 16 experimental groups. The orthogonal test was conducted by heating the blanks at a temperature between 880 and 950 °C (30–50 °C higher than A_{c3} to compensate for heat loss during transfer) for 3 to 6 min. Then, the plates were cooled in air for 5 s, before being transferred from the furnace to the stamping press. During this transfer, the plates lost a certain amount of heat to the air. The plates were placed in the stamping press for 40 s, and the die (the forming tool) closed on the sheet. Because the die is water-cooled, it rapidly extracts heat, quenching the steel into martensite while simultaneously shaping it. After quenching, the samples underwent hardness testing, room-temperature tensile testing, and microstructural analysis to evaluate their properties.

Hardness was measured using the Rockwell C scale (HRC). Indentations were made on polished sample surfaces, and the hardness values were averaged over five measurements per sample to ensure accuracy. Tensile strength was measured using a universal testing machine at ambient temperature using standardized specimens in accordance with the Standard Test Methods for Tension Testing of Metallic Materials E8/E8M, ASTM E8/E8M. The results were averaged across three specimens per group to minimize variability. The tests recorded yield strength, ultimate tensile strength, and elongation, with the results averaged across multiple samples to minimize variability.[12] Microstructural characterization was performed using optical microscopy and, where necessary, scanning electron microscopy. Samples were sectioned, mounted, ground, polished, and etched with an appropriate amount of nital solution to reveal the microstructure. The resulting images were analyzed to identify phases, grain size, and morphological features such as martensite laths or ferrite inclusions.[13]

Yield strength was obtained from the stress–strain curve. For steels without a distinct yield point, the 0.2% offset method was applied to determine the yield strength. Elongation was measured by marking the initial gauge length of the specimen before testing. After fracture, the two halves of the specimen were reassembled, and the final gauge length was measured. Elongation was then calculated as the percentage increase in length relative to the original gauge length. Area reduction was determined by measuring the minimum cross-sectional area at the fracture surface and comparing it with the original cross-sectional area of the specimen. The reduction of area was expressed as the percentage decrease in cross-sectional area. All procedures followed internationally recognized standards for the tensile testing of metallic materials, ensuring reproducibility and comparability of results.[14,15]

Young's modulus was determined from the initial linear portion of the tensile stress–strain curves obtained during testing. The slope of the elastic region provided the modulus values,

which were averaged across three specimens per group. For indentation tests, modulus values were estimated from the unloading portion of the force–penetration-depth curves using Oliver–Pharr analysis.[16]

3. Results

3.1 Orthogonal test results

Under the test conditions, all samples exhibited tensile strengths exceeding 1400 MPa and average hardness values above 450 HRC. Metallographic examination confirmed that the blanks had undergone complete martensitic transformation. Figure 1 shows the mechanical test data collected during the orthogonal experiments. The tensile curves were recorded using a universal testing machine, and the indentation curves were obtained from Rockwell C hardness tests using calibrated equipment. Each curve shows the elastic region, yield point (determined by the 0.2% offset method), tensile strength, and fracture behavior. The curves show consistent hardness response across samples, supporting the reported HRC values.

Hardness and strength increased with rising temperature, while tensile strength reached its maximum at a holding time of 4–5 min. Although water flow rate is generally proportional to strength, its effect on hardness and strength in this experiment was less pronounced owing to the heat storage capacity of the cooling platform. Nevertheless, a flow rate of 0.35 m/s was sufficient to satisfy quenching requirements. Range and variance analyses indicated that heating temperature was the dominant parameter affecting the hot stamping process, followed by holding time. The optimal process parameters were identified as a heating temperature of 930 °C, a holding time of 4–5 min, and a water flow rate of ≥0.75 m/s. Verification experiments

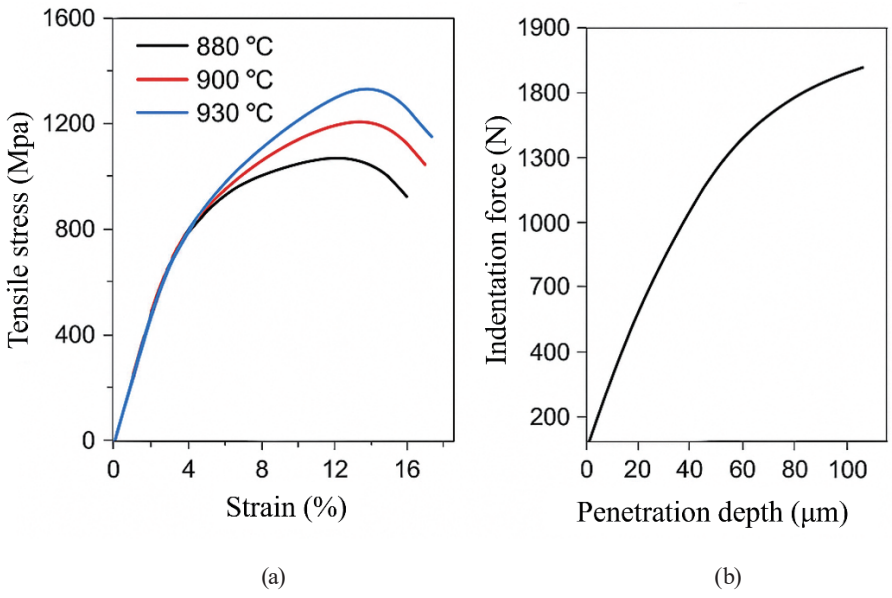

Fig. 1. (Color online) Mechanical test data for boron steel samples: (a) tensile stress–strain curves for samples tested at 880, 900, and 930 °C and (b) indentation force–penetration-depth curve from Rockwell C hardness testing.

conducted under these conditions produced an average hardness of 489 HRC and a tensile strength of 1535 MPa, with a uniform lath martensitic microstructure (Table 1).

The effect of each parameter on tensile strength was analyzed through the analysis of variance (Table 2). The heating temperature was the most significant parameter, followed by holding time. Although higher water flow rates generally improve cooling efficiency by ensuring that heat removal exceeds the steel's heat dissipation, the cooling water flow rate of 0.35 m/s was sufficient to achieve the required quenching rate of at least 27 ℃/s.

The measured Young's modulus values ranged between 205 and 215 GPa across all test groups, consistent with typical values for boron steels. No significant variation was observed with changes in heating temperature, holding time, or cooling water flow rate, indicating that boron segregation and martensitic refinement primarily affect strength and hardness rather than elastic stiffness. These results confirm that the elastic modulus remains stable, while tensile strength and hardness are strongly dependent on process parameters.

Table 1
Orthogonal test results.

Experiment group	Parameter			Result				
	Heating temperature (℃)	Holding time (min)	Water flow rate (ms/)	Hardness (HRC)	Tensile strength (MPa)	Yield strength (MPa)	Cross-sectional reduction (%)	Elongation (%)
1	880	3	0.75	48.46	1389.33	1237.67	7.7	15
2	880	4	1.13	47.99	1492.5	1278.5	7.9	11
3	880	5	1.55	48.2	1435	1316	8.53	16.03
4	880	6	0.35	48.58	1432	1308.67	9.03	19.37
5	900	3	1.13	48.28	1428	1285.67	8.23	18.27
6	900	4	0.75	47.93	1509.67	1378.67	9.33	12.37
7	900	5	0.35	48.14	1511.67	1354.33	10.27	14.3
8	900	6	1.55	47.62	1428.33	1318.67	9.27	12.1
9	930	3	1.55	46.83	1483	1324.3	10.13	13.1
10	930	4	0.35	47.11	1458.67	1341.67	8.27	11.83
11	930	5	0.75	47.83	1467.67	1290	9.83	13.57
12	930	6	1.13	46.62	1483	1304.67	8.67	19.5
13	950	3	0.35	47.42	1496	1374.33	10.5	8.67
14	950	4	1.55	46.57	1478.67	1357	8.43	14.93
15	950	5	1.13	46.85	1445.67	1296	9.7	20.83
16	950	6	0.75	46.63	1465.33	1308	10.07	11.37

Table 2
Analysis of variance results.

Parameter	Sum of squared deviations	Degree of freedom	F-value	F-critical value
Heating temperature (℃)	9637.372	3	1.757	6.990
Holding time (min)	6603.942	3	1.204	6.990
Water flow rate (m/s)	214.527	3	0.039	6.990
Error	16455.84	9	—	—

3.2 Microstructure and metallographic results

Figure 2 presents the martensitic microstructures obtained from the 16 orthogonal test groups described in Table 1. Each number corresponds to the orthogonal test groups listed in Table 1, which vary by heating temperature, holding time, and cooling water flow rate. Microstructures are shown at representative positions across the stamped blanks: undeformed regions, moderately deformed regions, and highly deformed regions. Within each group, microstructures were observed at three representative positions: (1) undeformed regions of the blank, (2) moderately deformed regions, and (3) highly deformed regions subjected to stamping. This clarification ensures that the figure is directly linked to the experimental design and highlights the effect of deformation on martensitic refinement.

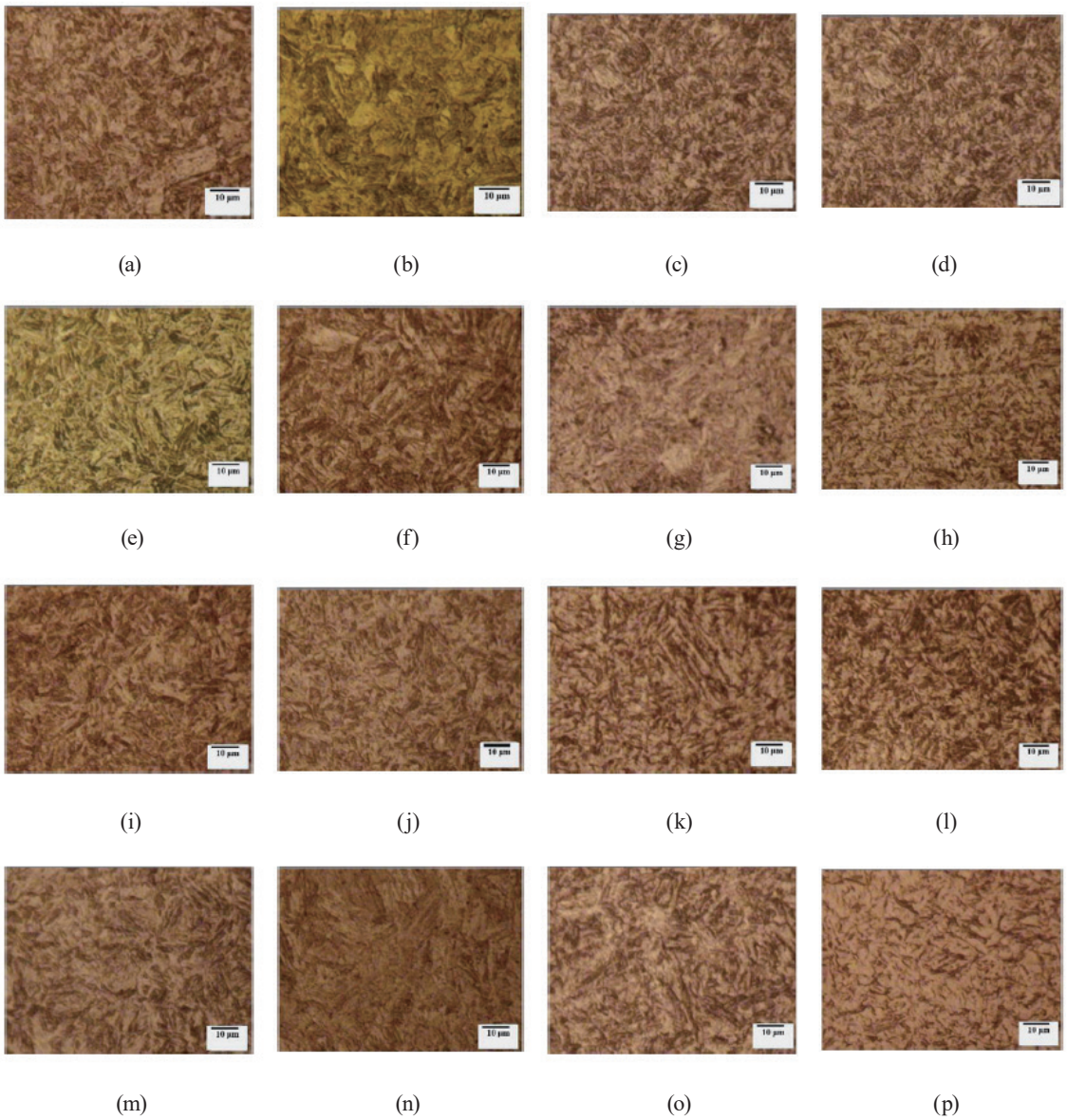

Fig. 2. (Color online) Metallographic microstructure of steel plate in each experimental group (the bar in the figures denotes 10 μm). (a) 1, (b) 2, (c) 3, (d) 4, (e) 5, (f) 6, (g) 7, (h) 8, (i) 9, (j) 10, (k) 11, (l) 12, (m) 13, (n) 14, (o) 15, and (p) 16.

In regions with little or no deformation, the martensitic structure appeared relatively coarse, with hardness values of 47.6 and 48.8 HRC, both below the average. In contrast, areas subjected to hot stamping deformation exhibited finer and more uniform martensite, with hardness values reaching 50.5 HRC. This improvement is attributed to the generation of dislocations, slip bands, and subgrain boundaries, which increase the effective grain boundary area. Deformation also fragments austenite grains, promotes dynamic recrystallization, and refines the microstructure, thereby enhancing mechanical properties.

Groups 4 (880 °C, 6 min, 0.35 m/s) and 7 (900 °C, 5 min, 0.35 m/s) exhibited incomplete martensitic transformation. In these samples, ferrite inclusions were observed alongside martensite, indicating that the cooling rate was insufficient to fully suppress ferrite formation. This mixed microstructure is what we define as incomplete martensitic transformation. In contrast, Groups 11 (930 °C, 5 min, 0.75 m/s) and 16 (950 °C, 6 min, 0.75 m/s) showed fully martensitic structures, meaning that the micrographs revealed a uniform lath martensitic phase without detectable ferrite or retained austenite. The distinction is therefore based on the presence or absence of secondary phases: incomplete transformation includes ferrite or retained austenite, while full transformation results in a homogeneous martensitic matrix (Fig. 3).

3.3 Performance improvement by hot stamping press

The performance improvements during stamping are achieved by the following mechanisms.

- High-temperature segregation: At elevated temperatures, boron segregates strongly to austenite grain boundaries, where it forms coherent boride phases. This segregation lowers grain boundary energy, obstructs dislocation motion, and impedes carbon diffusion. Collectively, these effects suppress the nucleation of proeutectoid ferrite and extend the incubation period.

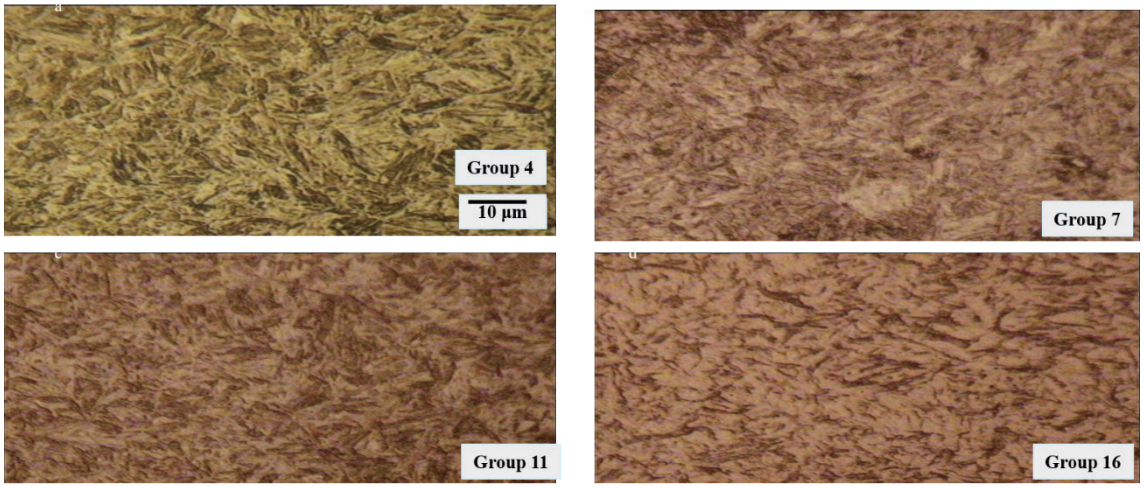

Fig. 3. (Color online) Metallographic structures of boron steel under different heat treatment conditions: (a) 880 °C, 6 min, 0.35 m/s; (b) 900 °C, 5 min, 0.35 m/s; (c) 930 °C, 5 min, 0.75 m/s; (d) 950 °C, 6 min, 0.75 m/s. The scale bar denotes 10 μm.

- Low-temperature inhibition: At lower temperatures, boron atoms substitute for iron atoms within the α-Fe lattice. This substitution causes lattice contraction and generates volumetric stress, which increases the energy barrier for phase transformation. As a result, the nucleation of proeutectoid ferrite embryos is suppressed, thereby enhancing the hardenability of the steel.
- Grain refinement: During hot stamping, the deformation of the steel fragments the existing austenite grains. This fragmentation promotes dynamic recrystallization, leading to the formation of finer austenite grains. Upon subsequent quenching, these refined grains transform into a martensitic microstructure with reduced grain size, which improves both strength and toughness.

Figure 4 shows comparative X-ray diffraction (XRD) spectra of boron steel samples taken from two distinct regions: a boron-rich region and a nonboron region. The horizontal axis shows the diffraction angle (2θ) ranging from 40 to 100 degrees, whereas the vertical axis represents the diffraction intensity. In the boron-rich region, the spectrum contains peaks corresponding to both α-Fe (alpha iron) and Fe_2B (iron boride). This indicates that boron has combined with iron to form boride phases in that part of the steel. In contrast, the nonboron region, shown in black, displays only peaks for α-Fe, confirming that no boron-related compounds are present there. The boron distribution in steel is uneven, with boron-rich areas forming distinct Fe_2B phases while other areas remain composed solely of α-Fe. This highlights how localized boron enrichment alters the steel's microstructure and phase composition.

Figures 5 and 6 present the experimental evidence of boron segregation during hot stamping. Figure 5(a) shows boron-rich aggregation regions at austenite grain boundaries, whereas Fig. 5(b) shows diffraction spots confirming coherent boride phases. Figure 5 shows SEM and electron diffraction images taken from boron-rich regions at austenite grain boundaries. The diffraction patterns indicate the formation of Fe_2B and FeB

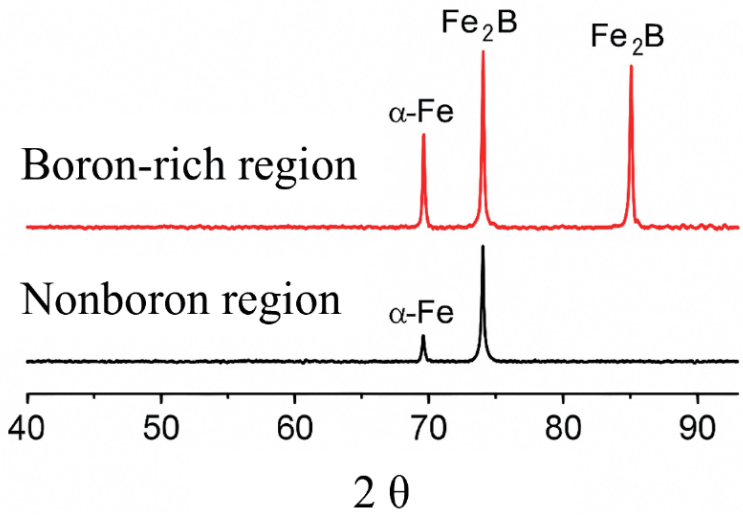

Fig. 4. (Color online) Comparative XRD spectra of boron steel samples taken from boron-rich and nonboron regions (this study).

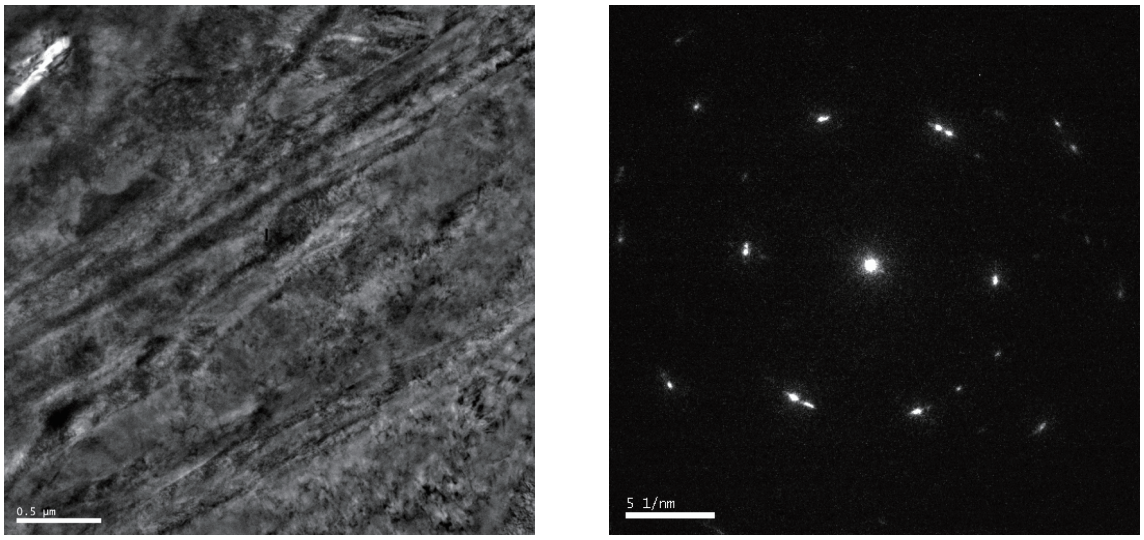

(a) (b)

Fig. 5. SEM image and electron diffraction pattern of boron-rich regions at austenite grain boundaries: (a) boron-rich aggregation region (the white bar denotes 0.5 μm) and (b) diffraction spots (the white bar denotes 1.0 μm).

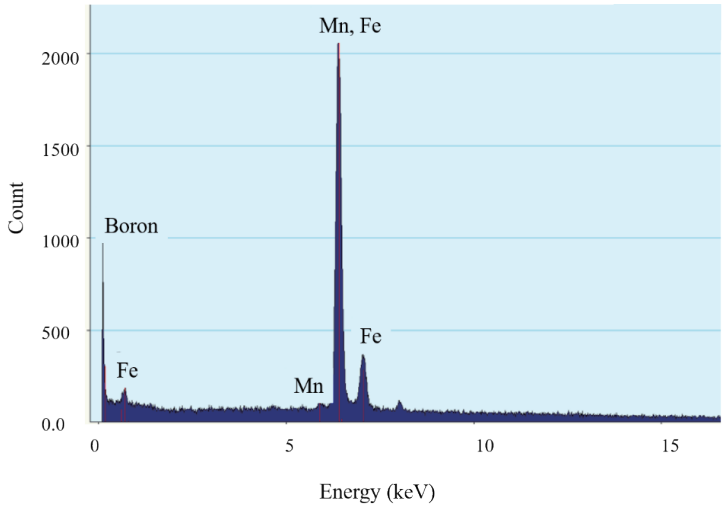

Fig. 6. (Color online) Energy spectrum of boron segregation sites.

borides, which are typical boron compounds in quenched boron steels. To further confirm phase identification, XRD profiles were collected from boron-rich regions and compared with nonboron regions. The XRD spectra revealed characteristic peaks corresponding to Fe_2B, whereas the nonboron regions showed only α-Fe peaks. Additionally, energy-dispersive X-ray (EDX) mapping was performed around the boron-rich sites, confirming the localized enrichment of boron at grain boundaries. These combined results provide direct evidence that boron segregation leads to the formation of Fe–B compounds, which

contribute to the suppression of ferrite nucleation and the stabilization of martensitic transformation.

Figure 5 shows SEM and electron diffraction images taken from boron-rich regions at austenite grain boundaries. To confirm the presence of boride phases, comparative XRD spectra were collected from boron-rich and nonboron regions. As shown in Fig. 5, the boron-rich region exhibits additional peaks corresponding to Fe_2B, whereas the nonboron region displays only αFe peaks. These results provide strong evidence of boron compound formation during heating. Figure 5 also shows the energy spectrum of boron segregation sites, demonstrating elevated boron concentration at grain boundaries. These results confirm that boron atoms preferentially segregate to grain boundaries during heating, forming boride phases that affect microstructural evolution. The performance improvements observed during stamping can be explained by the following mechanisms. First, at high temperatures, boron segregation lowers grain boundary energy and suppresses the nucleation of proeutectoid ferrite. Second, at lower temperatures, boron atoms substitute for iron atoms in the α-Fe lattice, generating volumetric stress that further inhibits ferrite nucleation. Third, grain refinement occurs during stamping deformation, fragmenting austenite grains and promoting dynamic recrystallization. Upon quenching, these refined grains transform into a finer martensitic microstructure, enhancing both strength and toughness.

Moreover, boron atoms hinder the diffusion of carbon at grain boundaries and occupy interstitial positions, making the nucleation of new phases during austenite transformation more difficult. These phenomena—boron segregation at grain boundaries, inhibition of carbon diffusion, and lattice contraction—collectively suppress the nucleation of new phases during the decomposition of austenite, thereby increasing the incubation period. When the temperature decreases, and pre-eutectoid ferrite embryos begin to form, boron atoms substitute for iron atoms in α-Fe, causing lattice contraction and increasing volumetric stress and strain, making it difficult for embryos to nucleate, thereby enhancing hardenability.

Figure 7 shows the martensitic microstructure at different positions of the part. In areas with little or no deformation, the martensitic microstructure is relatively coarse, with corresponding hardness values of 47.6 and 48.8 HRC, which are below the average hardness. In areas where the plates undergo hot stamping deformation, the microstructure becomes finer and more uniform, with a hardness value of 50.5 HRC, resulting in superior mechanical properties. This is attributed

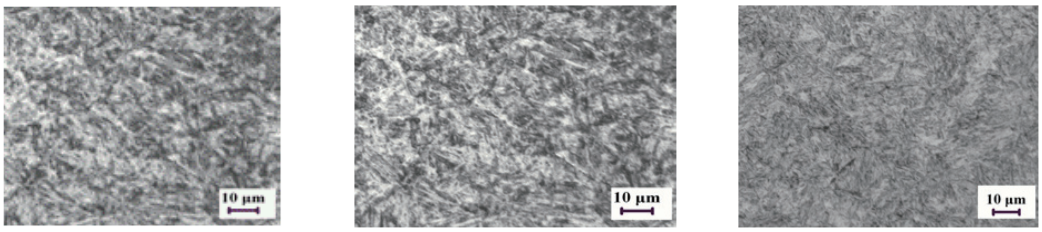

(a) (b) (c)

Fig. 7. Martensitic microstructure of hot stamping part: (a) undeformed microstructure, (b) microstructure with small deformation, and (c) microstructure with large deformation.

to the generation of a large number of dislocations, slip bands, and subgrain boundaries within the grains, which increases the effective grain boundary area. In comparison, deformation fragments the austenite grains, promotes dynamic recrystallization, and refines the grains, resulting in finer martensitic microstructures and enhanced mechanical properties of the part.

3.4 Real-time sensor-based process monitoring

In this study, the real-time sensor monitoring system was designed to control and optimize the three critical parameters, including heating temperature, holding time, and cooling water flow rate, during hot stamping. Heating temperature was controlled using a programmable furnace equipped with noncontact pyrometers, which continuously measured the blank's surface temperature to ensure it reached the target austenitization range (880–930 °C). Holding time was regulated by an automated timer linked to the furnace cycle, guaranteeing consistent exposure before transfer to the press. Cooling water flow rate was monitored and adjusted using embedded flow sensors within the die's cooling channels, ensuring that the quenching rate exceeded the threshold for martensitic transformation. Embedded piezoelectric force sensors detected volumetric expansion associated with phase transformation, while thermocouples measured die surface temperature to verify uniform cooling. These sensors provided real-time feedback to a closed-loop control system, which automatically adjusted process parameters to maintain optimal conditions and prevent defects.

The embedded piezoelectric force sensors were not exposed directly to the high-temperature blank (>1000 °C). Instead, they were installed beneath the die surface, in regions shielded by cooling channels and thermal insulation. In this configuration, the sensors operated at temperatures below 200 °C, well below their Curie temperature, ensuring stable functionality. Their role was to detect the pressure signatures and volumetric expansion associated with the martensitic phase transformation during quenching. Because martensitic transformation generates a measurable stress wave and expansion within the die cavity, the sensors captured these mechanical signals rather than direct thermal input. The data were then transmitted to the control system, which used the signal peaks to determine the onset and completion of phase transformation. Thus, the sensors functioned as indirect monitors of transformation kinetics, while pyrometers and thermocouples provided direct thermal measurements.

The blanks used in this study were cut from commercial boron steel sheets (22MnB5, 2 mm thickness). Each blank was prepared with the dimensions of 150 × 30 mm, polished to remove surface oxides, and cleaned with ethanol to eliminate contaminants before heating. The blanks were heated in a furnace to the target austenitization temperature (880–950 °C) for the specified holding times (3–6 min). After heating, the blanks were transferred to the stamping press within 5–8 s to minimize heat loss. This preparation ensured uniform initial conditions for all orthogonal test groups and allowed consistent evaluation of quenching and stamping performance.

The success of manufacturing HSS products hinges on the precise control of the thermal and mechanical process history, making the integration of advanced sensors into the die design a critical necessity for closed-loop quality assurance. While optimization and simulation provide

ideal parameters, real-time monitoring prevents costly die damage and guarantees the final microstructure.[17]

In the hot stamping process, sensors and noncontact devices are indispensable for monitoring the physical state of the die and the incoming for die protection and product quality verification. They must be installed to ensure correct material feed and position and the previous part's ejection to detect slugs or scraps that damage the die.[17,18] For the high-strength martensitic structure to form, the blank must maintain a specific cooling rate to pass the critical cooling curve.[19] Therefore, it is necessary to monitor the time–temperature history of the blank, the temperature of the die working surfaces, and the total quenching time, which are paramount.[18] Sensors must be embedded within the die surface to analyze pressure or volume changes in the material during quenching and precisely determine the exact moment the austenitic phase completely transforms into the desired martensitic structure.[19] Sensors enable the control system to automatically optimize the pressing (quenching) time piece by piece, ensuring optimal mechanical properties for 100% of the production and preventing defects such as incomplete phase transformation, which leads to reduced strength.[19]

The development of the quenching system and die geometry must be complemented by the integrated monitoring system. The feedback from these sensors provides essential data for rapid defect detection, process trending, and control algorithms for autonomous, high-quality manufacturing.[18]

4. Discussion

4.1 Effect of heating temperature and holding time

Analysis of the metallographic structures revealed that heating temperature and holding time significantly affect martensitic transformation. As heating temperature increases or holding time is extended, the martensite distribution tends to follow a normal distribution. When the holding time is too short or the heating temperature is too low, austenitization remains incomplete, resulting in limited improvement in hardenability. Conversely, excessive holding time or overly high heating temperature coarsens austenite grains, which in turn produces coarse martensite and an undesirable microstructure. Therefore, optimal values of both parameters are required to achieve a refined martensitic structure. On the basis of structural and mechanical property analyses, the optimal process conditions were identified as a heating temperature of 930 °C, a holding time of 4–5 min, and a water flow velocity of no less than 0.75 m/s.

To validate these parameters, two samples were tested under a heating temperature of 930 °C, a holding time of 4.5 min, and a water flow rate of 1.55 m/s. The measured average hardness was 489 HRC, and the average tensile strength reached 1535 MPa. Metallographic observations confirmed a uniform microstructure dominated by lath martensite (Fig. 8). The cooling rate during quenching exceeded the critical cooling rate of the material (15 °C/s), ensuring complete martensitic transformation and high strength.

In addition to strength and hardness, Young's modulus was evaluated from both tensile and indentation tests. The measured values ranged between 205 and 215 GPa across all test groups,

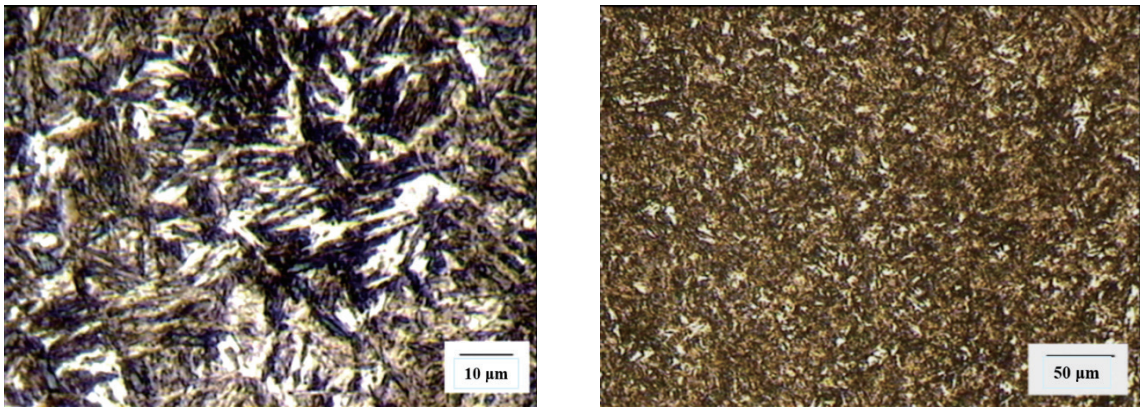

(a) (b)

Fig. 8. (Color online) Metallographic structure of martensite observed in samples (a) and (b).

consistent with typical boron steels. Importantly, no significant variation was observed with changes in heating temperature, holding time, or cooling water flow rate. This indicates that boron segregation and martensitic refinement primarily affect strength and hardness, whereas the elastic stiffness of the steel remains stable. These findings align with previous reports on boron-containing steels,[20] which confirms that modulus values remain within the typical range for martensitic steels, even as strength and toughness are enhanced.

4.2 Hot stamping press and blank-holder design

During hot stamping, the steel sheet is maintained at elevated temperatures, which facilitates deformation and reduces springback but also increases susceptibility to tearing and thinning. Consequently, blank-holder design plays a critical role in forming quality. Numerical simulations and experiments were conducted to evaluate the effect of blank holding on bumper beam stamping. The die gap was set to 1.18 times the sheet thickness, and blank-holding forces of 0, 30, and 300 kN were applied. Boundary conditions included an initial forming temperature of 850 °C, a friction coefficient of 0.12, and a stamping speed of 100 mm/s. The results showed that the maximum thinning rate exceeded that of the sample without blank holding, showing that the conditions are not appropriate. At forces above 300 kN, stamping cracks occurred in all samples (Fig. 9).

4.3 Die and quenching system design

A hot stamping die incorporating an edge-holding device was developed on the basis of the experimental results of this study (Fig. 10). The outer frame of the male and female dies served as the edge-holding mechanism, controlled by an ejection cylinder at the bottom of the press. The ejection force, adjusted for the device's weight, determined the effective blank-holding force. The crash beam hot stamping part was produced using semi-automated operation, with a manual feeding and unloading device. A simple die with bottom-support positioning was

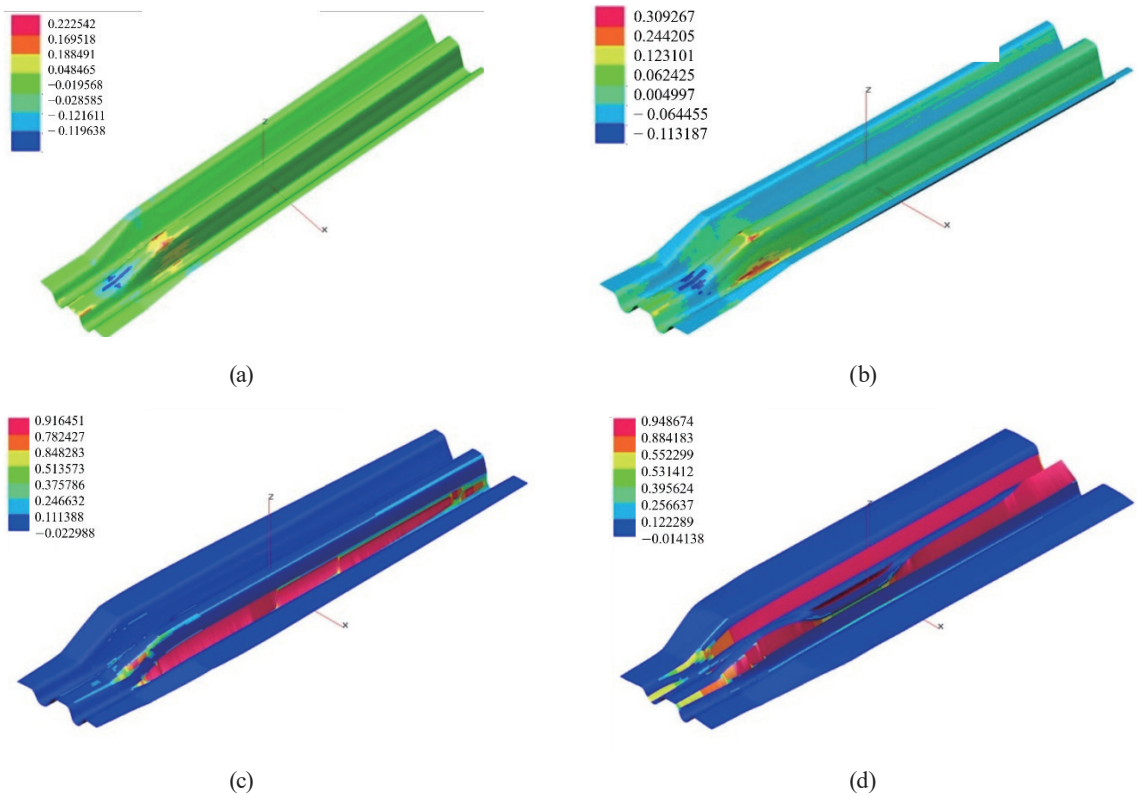

Fig. 9. (Color online) Edge compression simulation results for blank-holding forces of (a) 0 kN, (b) 30 kN, (c) 300 kN, and (d) 3000 kN.

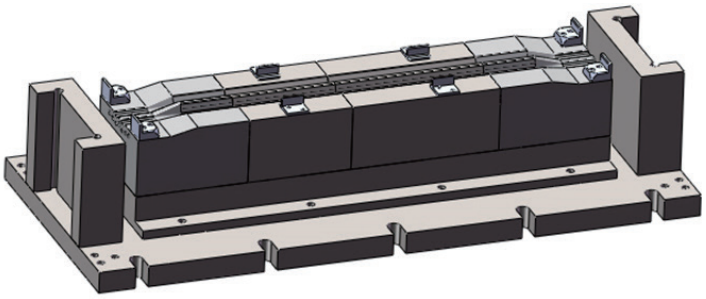

Fig. 10. (Color online) Heat stamping die design.

selected, considering the forming depth. The mold machining accuracy was set to Grade 6, and a rectangular guide device capable of withstanding high torque was employed. The clearance between male and female dies was determined from project research results obtained with the lower die structure.

The hydraulic press used had a working table size of 2400 × 1500 mm^2 with maximum and minimum open heights of 2000 and 500 mm, respectively. Considering blank dimensions, mold guidance, and installation space, the mold plan size was set at 1400 × 600 mm^2, with a closing height of 535 mm. Male and female molds were divided into four inserts each, with dimensions

designed to accommodate stress concentrations and deformation depth. A clearance coefficient of 1.18 tons was adopted, and mold clearance was set at 2.4 mm to account for thermal expansion. Mounting plates were designed to connect inserts to mold bases, integrate cooling circuits, and ensure sealing. An external cooling system was implemented, with adjacent inlet and outlet arrangements to improve the uniformity of cooling.

4.4 Process optimization

To minimize cracking defects, process parameters were optimized for the 2 mm boron steel 22MnB5. The recommended range included a heating temperature from 880 °C (above the A_{c3} transformation temperature of 811 °C) up to 930 °C, holding time of 4–5 min, forming speed of 35–100 mm/s, and initial forming temperature between Ac_1 and 900 °C. Preferred parameters were selected as 930 °C heating temperature, 4.5 min holding time, transfer time of 5–8 s (corresponding to an initial forming temperature of 800–850 °C), stamping pressure of 7 MPa, and stamping speed of 75 mm/s.

Die design parameters, including parting surfaces, die block division, clearance, and blank-holding devices, significantly affect stamping quality. Therefore, an excessively small clearance leads to severe thinning and tearing, whereas an overly large clearance reduces dimensional accuracy. In this study, parting surfaces were designed for ease of material placement, reliable positioning, and convenient removal. The die block lines were positioned to avoid regions of large geometric change, with upper and lower lines staggered to improve performance.

Parameters for quenching, including pipe diameter, spacing, depth, water flow rate, inlet temperature, and tank dimensions, were optimized to ensure quenching capability during continuous production. For 2 mm 22MnB5 steel, the selected parameters included a pipe diameter of 10 cm, spacing of 10 cm, depth of 5 cm, tank dimensions of 60 × 25 cm, inlet water temperature of 20–25 °C, and water flow rate ≥1.13 m/s. These conditions ensured that production cycle requirements were met and yielded stamped parts with martensitic content exceeding 95%.

4.5 Sensor selection and functionality

Sensors are required for monitoring the thermomechanical process during hot stamping. The required functions and parameters are summarized in Table 3.

Effective sensor placement enables active monitoring using the die. Sensors must be installed to withstand the high temperature, high pressure, and abrasive environment of hot stamping.[15] A high-speed pyrometer must be installed on the press frame to measure the blank's temperature immediately after it is placed in the lower die cavity. This measurement provides the initial forming temperature, ensuring that it remains above the critical A_{c3} transformation temperature. Type K thermocouples need to be installed 2–5 mm below the die's working surface. They must be positioned in parts of maximum heat accumulation, such as deep draw radii or areas distant from cooling channels, as well as near microstructural zones identified in simulations. The die temperature must remain below 200 °C for consistent quenching. Additional thermocouples or

Table 3
Sensor types, functions, and critical parameters for heat stamping die.

Sensor	Function	Monitoring parameter
Noncontact pyrometer	Measure the blank's temperature without physical contact, which is essential for monitoring the transfer and stamping phases.	Blank temperature and transfer time
Embedded thermocouples (type K or J)	Monitor the thermal stability of the die steel to ensure uniform and stable cooling conditions throughout the production run.	Die working surface temperature.
In-die piezoelectric/capacitive force/ pressure sensors	Directly measure the pressure and volume variation of the blank under compression. The pressure signature is used to confirm the completion of the martensitic phase transformation.	Phase transformation onset/ completion time and force consistency
Proximity/photoelectric sensors	Detect material and tooling position without contact, ensuring tool safety during stamping operations.	Strip/blank position, slug ejection, and die shut height

flow sensors need to be installed at the cooling channel inlets and outlets. These sensors verify that the cooling fluid maintains a consistent temperature and flow rate throughout the process.

Pressure sensors are permanently installed beneath the working surface of the lower die, particularly in regions with the slowest cooling rate, such as thick or geometrically complex sections of the part, for quality assurance. During rapid cooling, the transformation from austenite to martensite involves a slight volumetric expansion, which momentarily increases the pressure exerted on the die surface. By recording the time-resolved pressure curve, the system can detect the surge associated with martensitic transformation (M-finish).[21] The press is released only after this signal is detected, ensuring that the minimum required holding time for complete martensitic transformation is achieved.

Micron-level proximity sensors must be mounted on the die shoe to verify closure to the precise set-point, within approximately 0.001 mm, and prevent damage caused by debris, slugs, or misfed material.[22] Optical or through-beam sensors are positioned near the ejection area to confirm that the formed part is fully removed before the next cycle begins to prevent double-hit scenarios and ensure safe operation.

Data collected from sensors is integrated into a high-speed data acquisition system and a programmable logic controller. The data enables real-time process control, automated adjustments, and immediate shutdown in the event of defect detection.

5. Conclusions

We optimized the hot stamping parameters for boron steel 22MnB5 and developed a die design that can be integrated with advanced sensors, ensuring the reliable production of HSS parts. Experimental and simulation results showed that heating temperature is the most significant factor affecting the mechanical properties of hot-stamped components, followed by

holding time. The optimal process parameters were a heating temperature of 930 °C, a holding time of 4–5 min, and a sheet transfer time of 5–8 s. Under these optimized conditions, a tensile strength of 1535 MPa and a hardness of 48–50 HRC were achieved, with a microstructure composed of more than 95% uniform lath martensite. By designing a cooling system with a flow rate of at least 1.13 m/s, the quenching temperature is above the threshold of 15 °C/s for complete phase transformation. A blank-holding force of 30 kN or higher resulted in excessive thinning and cracking. To prevent defects, a simplified die design with sensors is proposed with a bottom-support structure and a clearance equal to 1.18 times the sheet thickness.

A multisensor monitoring system can be integrated into the designed hot stamping die. By embedding type K thermocouples and piezoelectric sensors, the pressure of the austenite-to-martensite transformation can be continuously monitored, transforming the die into an intelligent manufacturing tool. The system also enables the real-time verification of the quenching process, ensures complete martensitic transformation, and provides immediate defect prevention. The results of this research can be used for developing an optimization process for zero-defect HSS production.

References

1 M. Wang, Y. Li, Z. Wang, and E. Bao: J. Rare Earths **29** (2011) 489. https://doi.org/10.1016/S1002-0721(10)60485-1
2 J. Zhang, Y. Gao, J. Xing, S. Ma, D. Yi, L. Liu, and J. Yan: J. Mater. Eng. Perform. **20** (2011) 1658. http://link.springer.com/article/10.1007/s11665-010-9809-8
3 M. Carvalho, R. Xavier, C. Filho, C. Morone, M. Bocallini, and A. Sinatora: Iron Steelmaker **29** (2002) 27. https://www.researchgate.net/publication/279589433
4 H.-N. Li, S.-C. Han, B.-H. Zhang, G.-Y. Qiao, J.-B. Liu, and F. R. Xiao: Metall. Mater. Trans. A **54** (2023) 3271. https://doi.org/10.1007/s11661-023-07098-6
5 H. Fu, Q. Xiao, and J. Xing: Steel Res. Int. **77** (2016) 54. https://doi.org/10.1002/srin.200606131
6 H. Fu, Y. Qu, J. Xing, X. Zhi, Z. Jiang, M. Li, and Y. Zhang: J. Mater. Eng. Perform. **17** (2008) 535. https://doi.org/10.1007/s11665-007-9174-4
7 M. Kang and Y.-K. Lee: Metall. Mater. Trans. A **47** (2016) 3365. https://doi.org/10.1007/s11661-016-3536-1
8 M. Jung, M. Kang, and Y.-K. Lee: Acta Mater. **60** (2012) 525. https://doi.org/10.1016/j.actamat.2011.10.007
9 J. Zhou, B. Zhu, and J. Lin: J. Mater. Process. Technol. **212** (2012) 545. https://doi.org/10.1016/j.jmatprotec.2011.05.022
10 M. Malekian, M. G. Mostofa, S. S. Park, and M. B. G. Jun: J. Mater. Process. Technol. **212** (2012) 553. https://doi.org/10.1016/j.jmatprotec.2011.05.022
11 H. Jaafar, K. Mori, Y. Abe, and K. Nakanishi: J. Mater. Process. Technol. **227** (2016) 190. https://doi.org/10.1016/j.jmatprotec.2015.08.010
12 American Society for Testing and Materials: https://store.astm.org/standards/e8 (accessed December 2025).
13 American Society for Testing and Materials: https://store.astm.org/standards/e3 (accessed December 2025).
14 American Society for Testing and Materials: https://store.astm.org/e0008_e0008m-22.html (accessed December 2025).
15 International Organization for Standardization: https://www.iso.org/standard/78322.html (accessed December 2025).
16 W. C. Oliver and G. M. Pharr: J. Mater. Res. **7** (1992) 1564. https://doi.org/10.1557/JMR.1992.1564
17 Production Resources Inc.: https://www.production-resources.com/die-protection-sensors/ (accessed December 2025).
18 I. Wróbel and P. Danielczyk: Materials **11** (2023) 3658. https://doi.org/10.3390/ma16103658
19 R. Vollmer and C. Palm: Procedia Manuf. **29** (2019) 256. https://doi.org/10.1016/j.promfg.2019.02.135.
20 S. Kong, Z. Yu, X. Zhang, and Z. Zhang: J. Mater. Res. Technol. **30** (2024) 134. https://doi.org/10.1016/j.jmrt.2024.02.167

21 AZTERLAN: Patent No. EP3567126A1 (2019). https://www.azterlan.es/en/kh/system-and-method-of-quenching-monitoring-during-steel-hot-stamping.
22 AMETEK Landhttps: //www.ametek-land.com/-/media/ameteklandinstruments/documentation/industries/steel/ametek_land_pyrometer_temperature_measurement_cal_cgl_coating_line_rev3_en.pdf?la=en&revision=d62c05a7-3761-486f-b8ef-188a5a956795 (accessed December 2025).